Temperature Dependence of the NCl($a^1\Delta$) + I ($^2P_{3/2}$) Reaction from 300 to 482 K

Thomas L. Henshaw, Samuel D. Herrera, and L. A. (Vern) Schlie

Phillips Laboratory, Laser and Imaging Directorate, 3550 Aberdeen Ave., SE, Kirtland Air Force Base, New Mexico 87117

Received: August 25, 1997; In Final Form: May 18, 1998

The total quenching rate of NCl($a^1\Delta$) metastables by ground-state I($^2P_{3/2}$) atoms over the temperature range 297−473 K has been studied in a flow reactor. The room-temperature rate coefficient is $(2.1 \pm 0.4) \times 10^{-11}$ cm^3/(molecule s). In this temperature range, the temperature dependence for the total quenching rate is described by an Arrhenius expression of $k(T) = 1.1 \times 10^{-10} \exp(-519 \pm 143\ \mathrm{K}/T)$ cm^3/(molecule s). The rate coefficient for the energy transfer of NCl($a^1\Delta$) to I*($^2P_{1/2}$) at 300 K is $(1.5 \pm 0.7) \times 10^{-11}$ cm^3/(molecule s), which is in good agreement with a previous measurement. The magnitude of the energy transfer rate implies a large fraction of the I($^2P_{3/2}$) is converted to I*($^2P_{1/2}$), and the NCl($a^1\Delta$) + I($^2P_{3/2}$) reaction is an efficient source of I*($^2P_{1/2}$). Under the current experimental conditions, a simple kinetic model that simulated the experimental time histories of NF($a^1\Delta$) and NCl($a^1\Delta$) infers the Cl + N_3 rate coefficient of $(1.6 \pm 0.4) \times 10^{-11}$ cm^3/(molecules s) and is slower than previously measured.

Introduction

The $a^1\Delta$ state of NCl has recently received considerable attention as an energy carrier for a transfer laser operating on the I*($^2P_{1/2}$) → I($^2P_{3/2}$) spin−orbit transition at 1.315 μm.[1−5] Its importance stems from the efficient pumping of I*($^2P_{1/2}$) via collisions with NCl($a^1\Delta$) and ground state I($^2P_{3/2}$),

$$\mathrm{Cl} + \mathrm{N_3} \rightarrow \mathrm{NCl}(a^1\Delta) + \mathrm{N_2} \quad (1)$$

$$\mathrm{NCl}(a^1\Delta) + \mathrm{I}(^2P_{3/2}) \rightarrow \mathrm{I}^*(^2P_{1/2}) + \mathrm{NCl}(X^3\Sigma^-) \quad (2)$$

$$\mathrm{I}^*(^2P_{1/2}) \rightarrow \mathrm{I}(^2P_{3/2}) + h\nu\ (1.315\ \mu\mathrm{m}) \quad (3)$$

The subsequent observation of a population inversion between the I($^2P_{1/2}$−$^2P_{3/2}$) hyperfine states[2] and the photolytic laser demonstration[5] of an NCl($a^1\Delta$) to I($^2P_{3/2}$) energy transfer laser on based (2) and (3) warrants further investigation into the possibility of a purely chemically pumped I($^2P_{1/2} \rightarrow {}^2P_{3/2}$) laser.

For NCl($a^1\Delta$) to be practical as an energy source in chemical lasers, several issues need to be understood. Among these are the establishment of the most efficient chemical system for NCl($a^1\Delta$) generation of high NCl($a^1\Delta$) densities, the identification of rapid NCl($a^1\Delta$) quenching species, the self-annihilation rate of NCl($a^1\Delta$), the total rate constant and branching fraction of (2), and the NCl($a^1\Delta$) transport rates to the laser candidate species. Since F atoms typically initiate the production of Cl, N_3, and I in reactions 1 and 2, the system's capacity to generate NCl($a^1\Delta$) and I*($^2P_{1/2}$) is limited by the number of F atoms produced. In laboratory systems, the production of F atoms generally is facilitated through microwave or RF discharges of a dilute F-containing species such as CF_4 or F_2 in an inert bath gas in which the generated F atom density is usually limited to near 10^{13} atoms/cm^3. However, for larger, scaled-up chemical systems in which I*($^2P_{1/2}$) gain or laser demonstration measurements are desired a combustion system is usually required for producing 10^{16} F atoms/cm^3. Since a combustor operates at elevated temperatures up to 800 K, an investigation into the effects of heating on the NCl($a^1\Delta$) + I($^2P_{3/2}$) → I*($^2P_{1/2}$) + NCl($X^3\Sigma^-$) reaction must also be considered. In the only previous measurement, Bower and Yang[1] determined the total quenching rate constant of $k_Q \geq 1 \times 10^{-10}$ cm^3/(molecule s) for the NCl($a^1\Delta$) quenching by I($^2P_{3/2}$) at room temperature. This very rapid rate is interpreted as a near resonant energy transfer process:

$$\mathrm{NCl}(a^1\Delta, v' = 0) + \mathrm{I}(^2P_{3/2}) \rightarrow \mathrm{I}^*(^2P_{1/2}) + \mathrm{NCl}(X^3\Sigma^-, v'' = 2) \quad \Delta H = -50\ \mathrm{cm}^{-1} \quad (4)$$

In this study we report on the temperature dependence of the total quenching of NCl($a^1\Delta$) by I($^2P_{3/2}$) and discuss its implications for an NCl($a^1\Delta$) − I*($^2P_{1/2}$) chemical laser.

Experimental Section

The temperature dependence of the reaction between NCl($a^1\Delta$) metastables and ground-state iodine atoms I($^2P_{3/2}$) was investigated in a temperature-regulated discharge flow reactor. The flow reactor consists of a heated reaction zone where the metastables are produced and intensity−time profiles collected, a temperature regulated jacket for controlling the reaction temperature, and an optical detection system for monitoring the chemiluminescence of relevant species of interest. A diagram of the flow reactor is shown in Figure 1.

The reaction zone consists of a 130 cm long by 5.1 cm i.d. aluminum tube coated with Teflon (PTFE) to prevent the loss of radicals at the reactor walls. To facilitate efficient coating of the tube, the tube was divided into three sections. To maintain vacuum integrity, each section was joined together by means of a flange and a fluorocarbon-based polymer o-ring (Kalrez). Adjoining the reactor upstream is a 60 cm Teflon coated prereactor consisting of three 1.3 cm o.d. injection ports for adding F atoms and DCl to the reactor stream. The prereactor was not heated. The system was pumped by mechanical pump/Roots blower combination that produced linear flow velocities of 700−1100 cm/s at 0.8−1.0 Torr when throttled down by a ball valve. Time resolution is obtained by

S1089-5639(97)02760-6 CCC: $15.00
Published on Web 07/15/1998

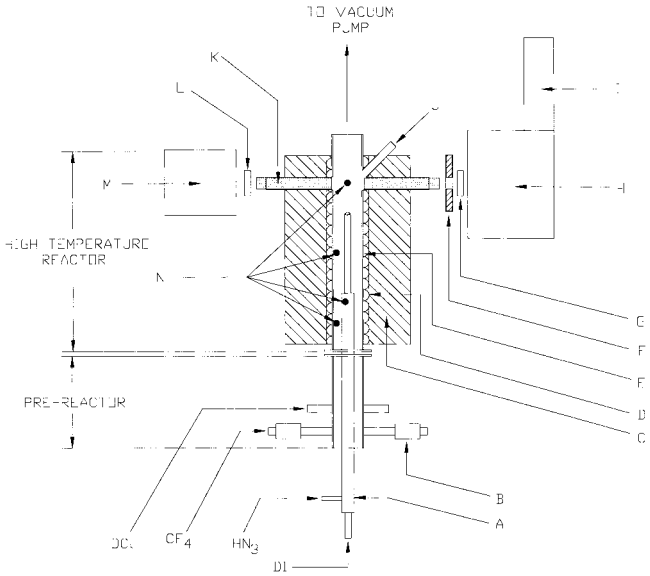

Figure 1. Experimental high-temperature flow reactor: A, concentric sliding injector; B, helical discharge; C, fiber insulation; D, nichrome heating coils; E, Teflon-coated aluminum reaction tube; F, light chopper; G, long pass filter; H, $^1/_8$ m monochromator; I, Ge detector; J, pressure port; K, polished quartz viewing rod; L, narrow band pass filter; M, S1 photomultiplier tube; N, thermocouples.

the use of two concentric sliding Pyrex injectors consisting of an outer 1.3 cm o.d. tube for injection of HN_3 and an inner 0.6 cm o.d. tube for dispensing the quencher species into the stream. Total reactor pressure was measured using a absolute capacitance manometer. Known amounts of reagents were introduced into the reactor by means of calibrated mass flow controllers.

Reactor heating is obtained by use of resistive heating of an 80−20 nickel−chrome (Nichrome) wire helically wound and encased in a ceramic jacket surrounding the reactor. The temperature is measured by inserting a thermocouple (type K, accuracy ±2°) just into the gas stream (about 0.3 cm) at three equally spaced points at 0, 45, and 90 cm from the observation point. A fourth temperature probe is inserted into the outer Pyrex injector near the exit port using a flexible thermocouple and thus provides a temperature measurement at the center of the tube. The heaters are regulated with a microprocessor based temperature feedback controller (Omega, model CN76000) integrating both the heater and thermocouple circuitry. The system's accuracy measured from center of the injector to the reactor walls ranged from ±1° at room temperature to ±7° at 480 K. The temperature dependence of this study is limited to 500 K, due to the thermal limits of the o-rings and the PTFE coating.

Optical observations are made perpendicular to the reactor tube through two ports consisting of a polished 17 cm long × 2.5 cm o.d. quartz rod to collect the various chemiluminescent emissions. $NCl(a^1\Delta)$ emissions for the kinetic analysis are isolated using a narrow band pass filter centered at 1075 nm (10 nm fwhm) and detected with an S1 photomultiplier tube (Hamamatsu R1767) cooled to −70 °C. The signals were then obtained by a computer data acquisition system for data processing. Spectral scans of $NCl(a^1\Delta)$ and $NF(a^1\Delta)$ for intensity measurements were corrected for detector (Hamamatsu R1767) and monochromator ($^1/_8$ m fl, 1 μm blaze, 600 grooves/mm grating) response via use of a calibrated tungsten halide standard lamp.[7] $I(^2P_{1/2})$ emission spectra (produced from the $NCl(a^1\Delta) + I(^2P_{3/2})$ reaction) were obtained by a $^1/_8$ m monochromator with a 1 μm grating (600 grooves/mm) and detected with a liquid nitrogen cooled Ge detector (ADC model 403L). The output of the Ge detector was then fed into a lock-in amplifier and recorded by computer data acquisition. Vibrationally excited $HF(X^1\Sigma^+,v'' = 3 \rightarrow 0)$ overtone emission near 875 nm was isolated with an 875 nm bandpass filter (100 nm fwhm) and detected with the aforementioned cooled S1 photomultiplier tube.

There are several potential chemical reaction schemes leading to the production of $NCl(a^1\Delta)$ including the $H + NCl_3$ and $N_2(X,v'') + ClN_3$ systems.[4,6] In this study, we use the following $F + DCl/HN_3/DI$ system:

$$F + DCl \rightarrow DF + Cl \quad (5)$$

$$F + HN_3 \rightarrow HF(v) + N_3 \quad (6)$$

$$F + DI \rightarrow DF + I \quad (7)$$

for the production of ground state Cl, N_3, and I followed by reactions 1 and 2 for $NCl(a^1\Delta)$ and $I^*(^2P_{1/2})$ generation. The use of the $Cl + N_3$ reaction for $NCl(a^1\Delta)$ generation is advantageous since the reaction is rapid[9] and is thought to produce a high yield.[8,10,11] However, to minimize the kinetic complications from the NCl bimolecular self-annihilation,[11] the $NCl(a^1\Delta)$ density is kept small by limiting the initial $[HN_3]_0$ density to $< 2 \times 10^{12}$ molecules cm^{-3}. Fluorine atoms are produced by flowing dilute mixtures of CF_4 in Ar into an RF discharge in the prereactor. The discharge was located about 45 cm upstream of the heated reactor. The RF discharge is a coaxial resonator with a helical inner conductor that generates a nominal resonant frequency of 8.5 MHz. An alumina tube of 20 cm long × 0.6 cm o.d. is placed in the center of the helical resonator through which CF_4 and Ar flow. The discharge is typically operated at 40 W forward power and <10 W reflected. Determinations of F atom density were made using a titration scheme involving the following reactions:[12]

$$F + C_2H_6 \rightarrow HF^*(v = 3) + C_2H_5 \qquad k = 8 \times 10^{-11}\ cm^3/(molecule\ s) \quad (8)$$

$$F + Cl_2 \rightarrow ClF + Cl \qquad k = 2.0 \times 10^{-10}\ cm^3/(molecule\ s) \quad (9)$$

The ethane was introduced into the reactor via the inner injector 2 cm from the observation point. The Cl_2 was injected 16 cm upstream from the observation point corresponding to about 21 ms of reaction time. The removal of F atoms by Cl_2 was tracked by the $HF(v = 3 \rightarrow 0)$ emission at 875 nm using an bandpass filter centered at this wavelength. Depending on the power and frequency, the typical conversion ratios are 0.2 F/CF_4 for low power (<40 W) and 1.0 F/CF_4 for high power, 70−100 W.

Chlorine atoms are produced by the $F + DCl \rightarrow Cl + DF$ reaction in the prereactor. Although the rate constant for this reaction is not known, the analogous $F + HCl$ reaction has a rate coefficient of 1.1×10^{-11} cm^3/(molecule s) and we would expect a similar rate constant magnitude.[13] The DCl is injected into the flow stream about 30 cm upstream from the heated reactor. Given a reaction time of 45 ms and reagent densities used here, the reaction has effectively gone to completion before it reaches the heated reaction zone and thus the Cl atom density is taken as the initial DCl density, $[DCl]_0$. The reaction of F with HN_3 is rapid[14] with $k = 1.1 \times 10^{-10}$ cm^3/(molecule s) with a yield of $N_3 \geq 0.9[HN_3]_0$. Ground-state I atoms are generated from the $F + DI \rightarrow I(^2P_{3/2}) + DF$ reaction. As with the $F + DCl$ reaction, the $F + DI$ rate constant is not determined; however, the $F + HI$ rate coefficient is $k = 8 \times 10^{-11}$ cm^3/

(molecule s) and the F + DI rate coefficient is also likely to be in this range.[15] Accordingly, the ground-state I density is taken as the initial DI density, $[DI]_0$. There are several reasons for the use of deuterium halide compounds. First, unlike vibrationally hot HF ($v = 2$), DF is off resonance with I*($^2P_{1/2}$) which helps minimize the congestion around the I*($^2P_{1/2}$) spectrum. Moreover, the use of DCl as a source of Cl atoms is more efficient at producing NCl($a^1\Delta$) metastables than microwave-discharged dilute Cl_2 mixtures.[16] Finally, the DF product formed from the F + DCl and DI reactions are apt to be a smaller quencher of NCl($a^1\Delta$) and I*($^2P_{1/2}$) than the products arising from other Cl and I source reactions such as the F + Cl_2, I_2, and ICl reactions.

Hydrogen azide was synthesized using a 10:1 molar excess of stearic acid over NaN_3 at 383 K under vacuum and stored as 5% mixture in Ar (Matheson, UHP, 99.9995%) in a stainless steel container. Argon carrier gas (Matheson, UHP), DCl (Isotec, 99.9%), DI (Cambridge, 99%), Cl_2 (10% Cl_2 in Ar, UHP), ethane (99.5%, Matheson), and O_2 (Matheson 99.5%) were used without further purification. The stock DCl and DI were diluted to 5 and 2.5% mixtures in Ar, respectively, and stored in 5 L Pyrex bulbs for the kinetic measurements.

Results and Discussion

NCl($a^1\Delta$) Formation and Decay in the Absence of I($^2P_{3/2}$). In order to measure the quenching of NCl($a^1\Delta$) by I($^2P_{3/2}$), measurements are made only after the maximum of the NCl($a^1\Delta$) intensity is reached to avoid kinetic complications with the formation rate of NCl($a^1\Delta$). In addition, having a large excess of F atoms can complicate the kinetic analysis by opening various competing side reaction channels. For example, the F + $N_3 \rightarrow$ NF($a^1\Delta$) + N_2 reaction has a rate constant[9,17] of (5 ± 2) $\times 10^{-11}$ cm^3/(molecule s) and a recent value of 3×10^{-11} cm^3/(molecule s) for the F + NCl($a^1\Delta$) quenching reaction[18] suggests these are significant N_3 and NCl($a^1\Delta$) removal processes. Thus attempts at keeping the F atom density to a minimum were undertaken by consuming excess F atoms through reactions with DCl and HN_3. Figure 2 shows typical NCl($a^1\Delta$) and NF($a^1\Delta$) emission time profiles resulting from the F/HN_3/DCl reaction system for the initial conditions $[F]_0 = 8.4 \times 10^{12}$ atoms/cm^3, $[HN_3]_0 = 2.2 \times 10^{12}$ molecules/cm^3, and $[DCl]_0 = 6.3 \times 10^{12}$ molecules/cm^3. On the basis of the long reaction time of the prereactor of 45 ms and an F + DCl rate constant of 1×10^{-11} cm^3/(molecule s), nearly all the DCl is converted to Cl atoms in the prereactor and the Cl density is taken as 6.3×10^{12} molecules/cm^3. The F atom density is then reduced proportionately to an amount given by the difference between the $[F]_0$ and $[DCl]_0$ densities. Accordingly, at the point where HN_3 is injected into the flow stream the $[HN_3]_0$ density is in slight excess over the F atom density. Since $[HN_3]_0$ reacts rapidly with F, most of the F atoms will be consumed in less than 5 ms by the F + HN_3 reaction. Thus the $[Cl] \gg [N_3] \approx [F]$ and the Cl + N_3 reaction should proceed relatively unhindered from any F atom initiated side reaction. Figure 3 shows a comparison of NCl($a^1\Delta$) and NF($a^1\Delta$) emission spectra corrected for detector/monochromator response[7] and arising from the flow conditions described above. The emission was dispersed with a $^1/_8$ m monochromator with 1 mm slits and a 1 mm blazed grating with 600 grooves/mm. The NCl($a^1\Delta$) and NF($a^1\Delta$) spectra were recorded at 20 and 9 ms, respectively, and spectral contamination from vibrationally excited HF is expected to be minimal. Integration of the emission intensities reveals the NCl($a^1\Delta$) band is about 2 times as intense as the NF($a^1\Delta$), which suggests the F + N_3 reaction is still prominent in the removal of N_3 despite the large excess of Cl atoms.

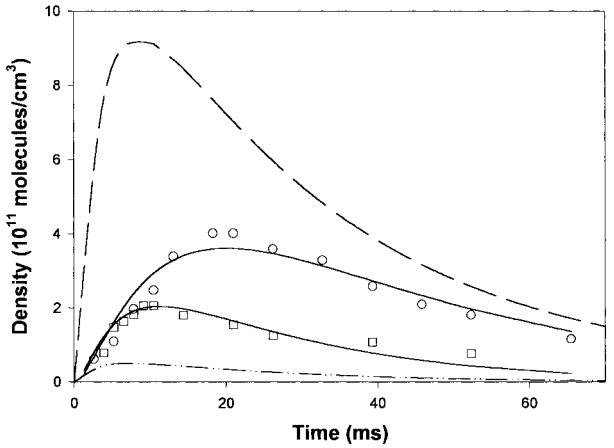

Figure 2. Time profiles for experimental NCl($a^1\Delta$) (○) and NF($a^1\Delta$), (□) intensity along the flow reactor for the following conditions: $[F]_0 = 2.2 \times 10^{12}$ molecules/cm^3, $[Cl]_0 = 6.3 \times 10^{12}$ molecules/cm^3, $[HN_3]_0 = 2.2 \times 10^{12}$ molecules/cm^3. The experimental NCl($a^1\Delta$) and NF($a^1\Delta$) intensities are scaled to the numerically calculated NCl($a^1\Delta$) and NF($a^1\Delta$) densities. The curves through these points are calculated from a least-squares fit of experimental data to a numerical model described in Table 1. A simulation of an NCl($a^1\Delta$) (− −) and NF($a^1\Delta$) (− ·· −) time profile using a much larger Cl + N_3 rate coefficient of $k = 1.5 \times 10^{-10}$ cm^3/(molecule s) is also shown. The increased NCl($a^1\Delta$) rise time and greatly diminished NF($a^1\Delta$) density do not support experimentally observed data.

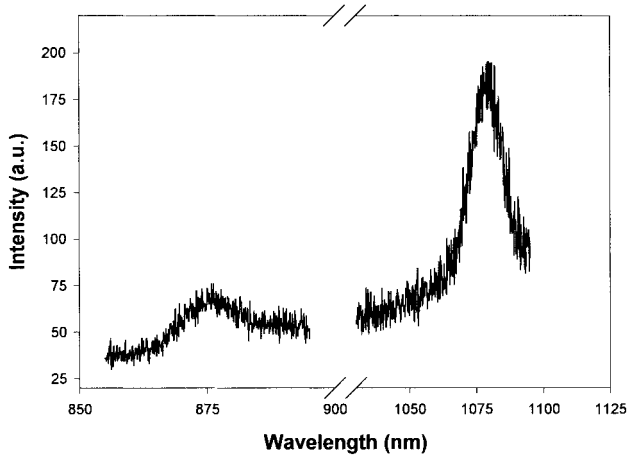

Figure 3. Chemiluminescent spectra of NCl($a^1\Delta$) and NF($a^1\Delta$) resulting from the conditions described in Figure 2. The spectra are corrected for detector and monochromator response. The integrated NCl($a^1\Delta$) emission intensity is about 2.5 times the NF($a^1\Delta$) emission.

Inspection of Figure 2 indicates the maximum NCl($a^1\Delta$) intensity occurs at about 20 ms, and on the basis of the previous rate coefficient for the Cl + N_3 reaction,[9] the rise time appears slower than anticipated. In an attempt to estimate the Cl + N_3 rate coefficient, a simple numerical model using kinetic information in Table 1 is constructed to simulate the observed NCl($a^1\Delta$) and NF($a^1\Delta$) time profiles shown in Figure 2. The calculated NCl($a^1\Delta$) and NF($a^1\Delta$) densities are obtained via numerical (stiff) integration of the coupled differentials listed in Table 1 and the experimental F, HN_3, and Cl densities described above. We note that while the F and HN_3 densities are experimentally derived, the Cl atom density is determined from the magnitude of the F + DCl reaction above. Although smaller Cl densities would be expected if an isotope effect were present, the reaction time is long enough to nearly facilitate complete conversion. In this vein, the loss of F and Cl atoms to reactor surfaces is also anticipated; however, they are assumed small on the Teflon surface.

TABLE 1: Room-Temperature Reactions and Rate Coefficients Used to Simulate the Time Profiles for NCl($a^1\Delta$) and NF($a^1\Delta$) in Figure 2

reacn	*k*, model Input	ref
1. $F + HN_3 \rightarrow N_3 + HF$	1.1×10^{-10} cm^3 molecules^{-1} s^{-1}	14
2. $Cl + N_3 \rightarrow NCl(a) + N_2$	1.4×10^{-11} cm^3 molecules^{-1} s^{-1}	this work
3. $Cl + N_3 \rightarrow NCl(b,X) + N_2$	2.8×10^{-12} cm^3 molecules^{-1} s^{-1}	this work
4. $F + N_3 \rightarrow NF(a) + N_2$	5.3×10^{-11} cm^3 molecules^{-1} s^{-1}	9, 14, 17
5. NCl(a) + NCl(a) $\rightarrow$ products	7.0×10^{-12} cm^3 molecules^{-1} s^{-1}	11
6. NF(a) + NF(a) $\rightarrow$ products	5.0×10^{-12} cm^3 molecules^{-1} s^{-1}	12
7. NCl(a) + F $\rightarrow$ products	3×10^{-11} cm^3 molecules^{-1} s^{-1}	18
8. NCl(a) + Cl $\rightarrow$ products	1×10^{-12} cm^3 molecules^{-1} s^{-1}	18
9. NCl(a) + DF $\rightarrow$ NCl(X) + DF	8×10^{-13} cm^3 molecules^{-1} s^{-1}	4
10. NF(a) + HF(v) $\rightarrow$ NF(b) + HF	1×10^{-12} cm^3 molecules^{-1} s^{-1}	19
11. NCl(a) $\rightarrow$ NCl(X)	32 s^{-1}	this work
12. NF(a) $\rightarrow$ NF(X)	42 s^{-1}	this work

The branching fraction of NF($a^1\Delta$) from the F + N_3 reaction is well established as ≥ 0.85.[14] Conversely, the Cl + $N_3 \rightarrow$ NCl($a^1\Delta$) + N_2 branching fraction is unknown. The yield of NCl($a^1\Delta$) is expected to be a function of where the repulsive triplet state of ClN_3 ($^3A''$), correlating to NCl($X^3\Sigma$) + N_2($X^1\Sigma$), crosses the singlet ClN_3 surface ($^1A'$), correlating to NCl($a^1\Delta$) + N_2($X^1\Sigma$). In particular, it is the position of this curve crossing in relation to the barrier for ClN_3 ($^1A'$) $\rightarrow$ NCl($a^1\Delta$) + N_2 ($X^1\Sigma$) dissociation that determines the yield of NCl($a^1\Delta$). In the analogous HN_3 anf FN_3 species, the positions of the singlet−triplet surface crossings are significantly different and, consequently, so are the yields of NF($a^1\Delta$) and NH($a^1\Delta$). In FN_3 (X^1A'), the F−N_3 bond is stronger than the FN−N_2 bond and the molecule is expected to dissociate to NF($a^1\Delta$) and N_2($X^1\Sigma$). An *ab initio* calculation for this barrier gives a height of about 3844 cm^{-1} and a triplet surface crossing lying outside the barrier on the product side.[8] Since the triplet surface crosses the singlet surface only once upon dissociation, the probability of NF changing state is low and the thermal NF($a^1\Delta$) branching fraction approaches unit. Conversely, in HN_3 the H−N_3 and HN−N_2 bonds are about equal and the magnitude of the barrier to NH($a^1\Delta$) + N_2($X^1\Sigma$) dissociation is about 1200 cm^{-1}. However, the triplet crossing lies well inside of the barrier and HN_3 traverses the crossing point many times before surmounting the barrier so the probability of singlet−triplet crossing increases.[19] Thus, one expects thermal dissociation to yield primarily NH($X^3\Sigma$) and N_2($X^1\Sigma$), and indeed, this is experimentally confirmed.[20,21] For ClN_3, the Cl−N_3 bond is probably stronger than the ClN−N_2 bond and the singlet channel is preferred energetically. In an *ab initio* calculation for ClN_3, the triplet crossing lies at the top of the barrier (5444 cm^{-1})[22] and the ClN_3 branching fraction lies probably somewhere between HN_3 and FN_3. To that end, the sensitivity of the NCl($a^1\Delta$) branching fraction in regard to the observed time profile is examined within the model.

The removal of NCl($a^1\Delta$) and NF($a^1\Delta$) by second-order processes include the bimolecular self-annihilation reactions,

$$NCl(a^1\Delta) + NCl(a^1\Delta) \rightarrow \text{products} \qquad k = 7.1 \times 10^{-12}\ \text{cm}^3/(\text{molecule s})^{11} \quad (10a)$$

$$NF(a^1\Delta) + NF(a^1\Delta) \rightarrow \text{products} \qquad k = 5.0 \times 10^{-12}\ \text{cm}^3/(\text{molecule s})^{12} \quad (10b)$$

and the Cl/F + NCl($a^1\Delta$) reactions.[18] Other bimolecular channels include the DF quenching of NCl($a^1\Delta$). The value of the DF + NCl($a^1\Delta$) rate coefficient is assumed to be of similar magnitude, $k = 8 \times 10^{-13}$ cm^3/(molecule s), to the analogous HF + NCl($a^1\Delta$) reaction.[4] Since vibrationally excited HF(v) is produced via the F + HN_3 reaction, the pooling reaction of HF(v) + NF($a^1\Delta$) $\rightarrow$ NF($b^1\Sigma^+$) is incorporated as a removal process for NF($a^1\Delta$).[23] The radiative lifetime for NF($a^1\Delta$)[24] is generally accepted as 5 ± 1 s. In contrast, the radiative lifetime for NCl($a^1\Delta$) is not accurately known as previous measurements and calculations have put the radiative lifetime in the range of $1.4 < \tau_{NCl(a)} < 5$ s.[8,25−27] Other first-order NCl($a^1\Delta$) losses include a pseudo-first-order quenching by Ar, $k \leq 1 \times 10^{-15}$ cm^3/(molecule s),[4] and a nonradiative first-order (diffusional) loss. Since many of these NCl($a^1\Delta$) first-order rates are undetermined, these processes are combined into a single first-order loss rate. The first-order NF($a^1\Delta$) losses are also treated in this manner.

Comparisons of the calculated and experimental time profiles are made by scaling the response corrected peak experimental intensity data to the maximum calculated densities. Extraction of the rate coefficients are determined by keeping the known rate coefficients in Table 1 such as the F + HN_3/N_3 reactions fixed while varying the Cl + N_3 branching reaction and first-order NCl($a^1\Delta$) loss parameters until a best fit is achieved. The NCl($a^1\Delta$) branching fraction was estimated by varying the Cl + $N_3 \rightarrow$ NCl(a,b,X) branching reaction for several conditions ranging from 0.2 to 1.0 and comparing the fit to the experimental data. When the NCl($a^1\Delta$) and NF($a^1\Delta$) rise times begin to depart from observed values (the experimental t_{max} lies at approximately 20 and 9 ms, respectively), or the ratio of [NCl(a^1D)] to [NF(a^1D)] begins to diverge from experimental observation (the relative integrated NCl($a^1\Delta$)/NF($a^1\Delta$) intensity ratio at t_{max} is about 2.5 ± 0.5), the limit of the branching fraction is obtained. For example, a rate coefficient of 1.4×10^{-11} cm^3/(molecule s) is assigned to reaction 2 in Table 1 along with the appropriate rate coefficient value for reaction 3 to yield NCl($a^1\Delta$) branching fractions of 1.0, 0.85, 0.75, 0.70, 0.65, 0.5, and 0.25. Figure 4 illustrates the sensitivity of the branching fraction to the analysis fit. For purposes of clarity, only the NCl($a^1\Delta$) branching fraction (ϕ_a) cases for 0.7 and 0.5 are shown. In keeping with the observed relative NCl($a^1\Delta$)/NF($a^1\Delta$) ratio, the curve for an NCl($a^1\Delta$) branching fraction of 0.7 represents the lower limit of the Cl + $N_3 \rightarrow$ NCl($a^1\Delta$) + N_2 product channel. For conditions where the $\phi_a < 0.7$ there is a marked drop off in the NCl($a^1\Delta$)/NF($a^1\Delta$) ratio and increased rise times that are inconsistent with observed time profiles. This is clearly seen in the $\phi_a = 0.5$ case in Figure 4, where the rise time is substantially faster ($t_{max} = 16$ ms) and the NCl($a^1\Delta$)/NF($a^1\Delta$) ratio is significantly reduced. In this manner, the rate coefficients for reaction 2 in Table 1 were then systematically varied over a magnitude from 1.0×10^{-11} to 2.4×10^{-11} cm^3/(molecules s) in conjunction with reaction 3 to give NCl($a^1\Delta$) branching fractions ranging from 0.2 to 1.0.

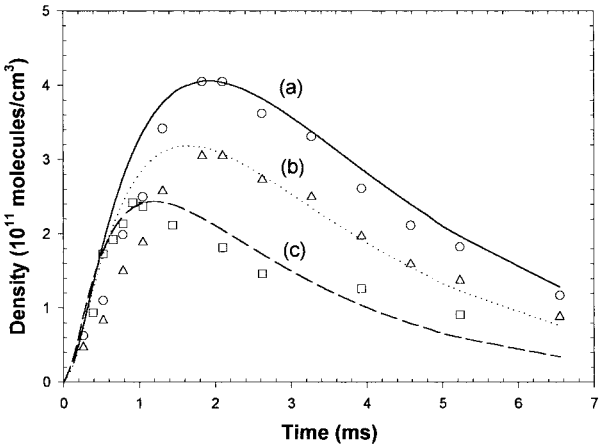

Figure 4. Sensitivity of the model to the NCl($a^1\Delta$) branching fraction using a Cl + N_3 → NCl($a^1\Delta$) + N_2 rate coefficient of 1.4×10^{-11} cm^3/(molecules s) and various rate coefficients for the Cl + N_3 → NCl($b^1\Sigma$, $X^3\Sigma^-$) + N_2 reaction to yield NCl($a^1\Delta$) branching fractions of 0.7 and 0.5. Time profiles: (a) (—) calculated NCl($a^1\Delta$) time profile with a branching fraction of 0.7, (○) experimental NCl($a^1\Delta$) time profile scaled to a branching fraction of 0.7; (b) (•••) calculated NCl($a^1\Delta$) time profile with a branching fraction of 0.5, (△) experimental NCl($a^1\Delta$) time profile scaled to a branching fraction of 0.5; (c) (- - -) calculated NF($a^1\Delta$) time profile with a branching fraction of 1.0, (□) experimental NF($a^1\Delta$) scaled to a branching fraction of 1.0. In this series, the curve for the 0.7 branching fraction case represents the lower limit of the NCl($a^1\Delta$) branching fraction.

It turns out that the observed NCl($a^1\Delta$) time profile data is best simulated to a Cl + N_3 → NCl($a^1\Delta$) + N_2 rate coefficient of $(1.6 \pm 0.4) \times 10^{-11}$ cm^3/(molecules s) with a corresponding branching fraction ≥0.7. We note that Benard and co-workers measured the yield of NCl($a^1\Delta$) to be near unity in a thermal decomposition of ClN_3 from the sensitized heating of SF_6/ClN_3 mixtures via laser photolysis at 10.6 μm.[8]

Other NCl($a^1\Delta$) and NF($a^1\Delta$) production and removal processes in Table 1 were tested for their sensitivity to changes in rate coefficients and reagent densities by varying the parameter inputs into the model. For example, a 2-fold increase in the NCl($a^1\Delta$) first-order rate coefficient reduces the peak NCl($a^1\Delta$) by 20%. A 30% increase in $[F]_0$ atoms causes a 65% increase in the peak NF($a^1\Delta$) density while reducing the NCl($a^1\Delta$) peak density by 10%. Similarly, increasing the $[Cl]_0$ atoms by 30% increases the [NCl($a^1\Delta$)] by 20% and reduces the NF($a^1\Delta$) density by 20% while reducing the time for NCl($a^1\Delta$) to reach its maximum density by 5 ms.

A simulation of the time profile is shown in Figure 2 for the conditions described in Table 1 by the solid line drawn through these data points. A best fit of calculated data to the experimental data infers a rate constant and branching fraction of about 1.4×10^{-11} cm^3/(molecule s) and 0.75, respectively, for the Cl + N_3 → NCl($a^1\Delta$) + N_2. These values are comparable with the recent values of $(2.2 \pm 0.2) \times 10^{-11}$ cm^3/(molecule s) and 0.5 ± 0.2 obtained by Setser and co-workers.[18] For contrast, the model is run with a much more rapid Cl + N_3 rate constant of 1.5×10^{-10} cm^3/(molecule s) that approximates the value given by Liu and Coombe.[9] The results are shown in Figure 2 where the maximum NCl($a^1\Delta$) density appears much earlier in time than the experimental determined data while the NF($a^1\Delta$) density is reduced substantially. In view of the delayed rise time of NCl($a^1\Delta$) and the appearance of NF($a^1\Delta$), the current data suggest the Cl + N_3 rate is slower than previously reported.

Temperature Dependence of the NCl($a^1\Delta$) + I($^2P_{3/2}$) Reaction. The quenching of NCl($a^1\Delta$) with added quencher species Q in the absence of secondary second-order processes is described by the following set of reactions:

$$\mathrm{NCl}(a^1\Delta) + \mathrm{Q} \rightarrow \mathrm{NCl}(X) + \mathrm{Q}^* \quad k_{Qa} \tag{11a}$$

$$\rightarrow \mathrm{NCl}(X) + \mathrm{Q} \quad k_{Qb} \tag{11b}$$

$$\rightarrow \text{products} \quad k_{Qc} \tag{11c}$$

$$\mathrm{NCl}(a^1\Delta) \rightarrow \mathrm{NCl}(X) + \mathrm{hv} \quad k_r \tag{12}$$

$$\mathrm{NCl}(a^1\Delta) \rightarrow \mathrm{NCl}(X) \quad k_w \tag{13}$$

where k_{Qa} is quenching involving energy transfer, k_{Qc} is reactive quenching and $k_Q = k_{Qa} + k_{Qb} + k_{Qc}$ is the total quenching rate constant, k_r is the radiative rate, and k_w is the wall removal rate of NCl($a^1\Delta$). Thus the loss of NCl($a^1\Delta$) in the system in the presence of added quencher is

$$\frac{-\mathrm{d}[\mathrm{NCl}(a^1\Delta)]}{\mathrm{d}t} = (k' + k_Q[Q])[\mathrm{NCl}(a^1\Delta)] \tag{14}$$

where k' is the sum of all first-order loss processes. Under pseudo-first-order quenching, the integrated rate expression becomes

$$\ln[\mathrm{NCl}(a)] = -(k_Q[Q] + k')t \tag{15}$$

where [NCl($a^1\Delta$)] is the relative NCl($a^1\Delta$) signal and t is the reaction time given by d/v, where d is the distance between the observation point and the quencher inlet and v is average linear velocity of the reagent flow. The quenching of NCl($a^1\Delta$) by I($^2P_{3/2}$) at elevated temperatures proceeds similarly to 300 K quenching except that the reaction times and reagent density decrease with temperature. Accordingly, temperature corrections to the flow velocity are made as follows

$$v = \left(\frac{T_r}{273}\right)\left(\frac{P_r}{760}\right)\left(\sum_i f_i/A\right) \tag{16}$$

where P_r is the reactor total pressure in Torr, T_r is the reactor temperature in K, A is the cross sectional area of the flow tube, and $\sum f_i$ the total flow rate. Similarly, the temperature correction to the reagent density is given as

$$\rho_i = 3.2 \times 10^{16} P_r (f_i / \sum_i f_i)(298/T_r) \tag{17}$$

where ρ_i is the reagent density and f_i is the individual flow rate of the reagent species. Quenching measurements are made with the outer injector, where HN_3 is added to the reactor stream, fixed at about 60 ms upstream from the observation point. Due to the rise time of Cl + N_3, the actual reaction time for the NCl($a^1\Delta$) + I reaction is reduced to about 40 ms with typical measurements taken in the 15−35 ms range. The total quenching rate constant k_Q is obtained by plotting changes in relative NCl($a^1\Delta$) intensity vs Q at fixed reaction time:

$$\left(\frac{\partial\{\ln[\mathrm{NCl}(a^1\Delta)]\}}{\partial \mathrm{Q}}\right)_t \tag{18}$$

As a reference reaction, the NCl($a^1\Delta$) + O_2 total quenching rate constant was measured since this was previously determined by three groups, Clyne et al.,[10a] Coombe et al.,[4] and recently by Setser et al.[18] The consensus for k_Q by O_2 is in the range of $(2-5) \times 10^{-12}$ cm^3/(molecule s). In comparison, the quenching

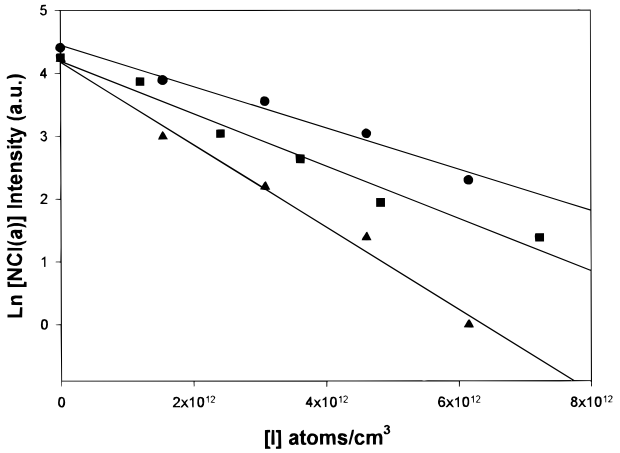

Figure 5. Typical quenching plot for the removal of $NCl(a^1\Delta)$ by ground-state I atoms for three reaction times of 19.3, 25.7, and 32.2 ms at room temperature. For these data, the reagent starting densities are $[F]_0 = 1.7 \times 10^{13}$ atoms/cm^3, $[DCl]_0 = 7.8 \times 10^{12}$ molecules/cm^3, and $[HN_3]_0 = 2.1 \times 10^{12}$ molecules/cm^3. The line drawn through these points is a least-squares fit to the data. Several independent quenching measurements were made giving an average room temperature value of $(2.1 \pm 0.4) \times 10^{-11}$ cm^3/(molecule s).

measurements made here give a total quenching rate constant of $(2.1 \pm 0.5) \times 10^{-12}$ cm^3/(molecule s), in agreement with the previous measurements.

A typical quenching plot for the removal of $NCl(a^1\Delta)$ by ground-state I atoms for three reaction times of 19.3, 25.7, and 32.2 ms at room temperature is shown in Figure 5. For these data, the reagent starting densities are $[F]_0 = 1.7 \times 10^{13}$ atoms/cm^3, $[DCl]_0 = 7.8 \times 10^{12}$ molecules/cm^3, and $[HN_3]_0 = 2.1 \times 10^{12}$ molecules/cm^3. The DI, hence I atom density, is held in excess over the limiting reagent, HN_3, and pseudo-first-order kinetics with $[I] > [NCl(a^1\Delta)]$ is implied from the linearity of the plot. Further, since all the decay curves extrapolate to a single point, the quenching of $NCl(a^1\Delta)$ is associated with the addition of I and not the decay of a precursor species. The slope of each curve gives $k_Q\Delta t$, which for the reaction times given provides an average total quenching rate constant of $(1.8 \pm 0.4) \times 10^{-11}$ cm^3/(molecule s). Several quenching measurements were made giving an average room temperature value of $(2.1 \pm 0.4) \times 10^{-11}$ cm^3/(molecule s).

In a similar vein, experiments were directed at measuring the specific energy transfer rate coefficient, k_{Qa}, for the energy transfer of $NCl(a^1\Delta)$ to $I^*(^2P_{1/2})$ at room temperature,

$$NCl(a^1\Delta) + I(^2P_{3/2}) \rightarrow I^*(^2P_{1/2}) + NCl(X^3\Sigma^-) \quad (19a)$$

It is assumed that $I^*(^2P_{1/2})$ nonradiative losses and quenching by all other reactor species are small so that the observed $I^*(^2P_{1/2})$ emission equals the rate of formation from $NCl(a^1\Delta)$. Figure 6a is a time profile of the I* emission formed over the first 40 ms with $[F]_0 = 1.6 \times 10^{13}$ atoms/cm^3, $[DCl]_0 = 5.6 \times 10^{12}$ molecules/cm^3, $[HN_3]_0 = 1.4 \times 10^{12}$ molecules/cm^3, and $[DI]_0 = 6.3 \times 10^{12}$ molecules/cm^3. Under these conditions, the $[I] > [NCl(a^1\Delta)]$ and pseudo-first-order conditions are maintained. The energy transfer rate of I* is obtained from a least-squares fit of the data to a first order formation of the form $I(t) = a + b(1 - \exp(-kt))$ and is shown in Figure 6a. Several measurements of the formation rate of I* were made as a function of I atom density and are shown in Figure 6b where the error bars in each data point represents the uncertainty (2σ) of the least-squares fit. The slope of the line from a least-squares fit gives an $NCl(a^1\Delta)-I^*$ energy transfer rate of (1.5 ± 0.9) $(2\sigma) \times 10^{-11}$ cm^3/(molecule s) and is in agreement with the previous measurement by Ray and Coombe of $(1.8 \pm 0.3) \times 10^{-11}$ cm^3/(molecule s).[3]

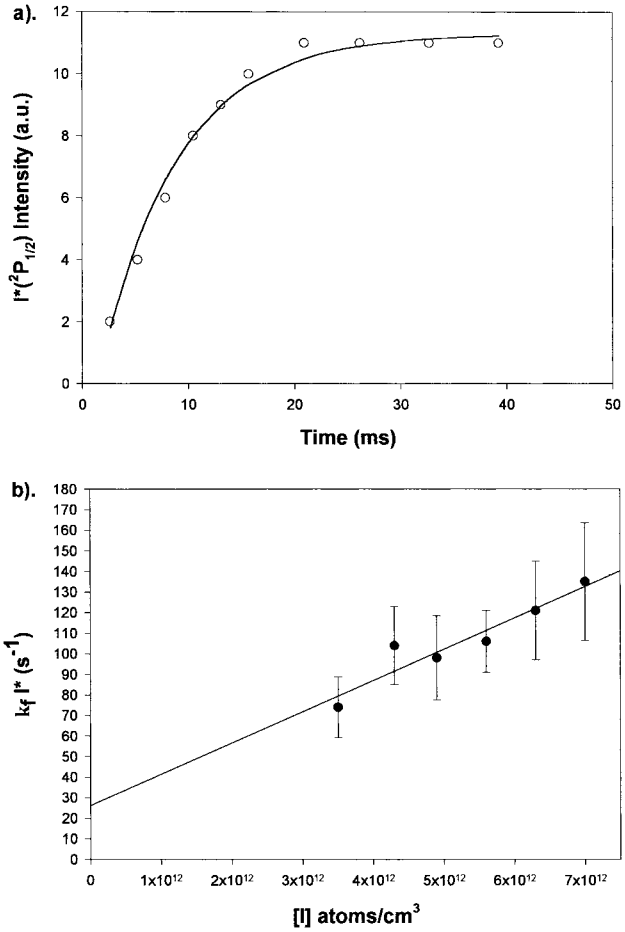

Figure 6. (a) Time profile of the $I^*(^2P_{1/2})$ emission formed over the first 40 ms with $[F]_0 = 1.6 \times 10^{13}$ atoms/cm^3, $[DCl]_0 = 5.6 \times 10^{12}$ molecules/cm^3, $[HN_3]_0 = 1.4 \times 10^{12}$ molecules/cm^3, and $[DI]_0 = 7.0 \times 10^{12}$ molecules/cm^3. The line drawn through the data points is calculated from a least-squares fit of the data to a first-order formation rate of the form $I(t) = a + b(1 - \exp(-kt))$. (b). A least-squares fit of the formation rates obtained as a function of added $I(^2P_{3/2})$ density. The slope of the line from a least-squares fit gives an $NCl(a^1\Delta)-I^*$ energy transfer rate of (1.5 ± 0.9) $(2-) \times 10^{-11}$ cm^3/(molecule s).

Figure 7 shows two typical quenching plots for $NCl(a^1\Delta)$ by $I(^2P_{3/2})$ at 345 and 448 K. At 345 K, $k_Q = (2.6 \pm 0.5) \times 10^{-11}$ cm^3/(molecule s), and at 448 K, $k_Q = (4.1 \pm 0.6) \times 10^{-11}$ cm^3/(molecule s), where the uncertainties here accrue predominantly from errors in gas temperature, chemiluminescent intensity, and the error in determining the slope $\delta\{\ln[NCl(a)]\}/\delta Q$. The rate coefficient data over the temperature range of 300−482 K is summarized in Table 2 where these data reflect a small positive change in the total quenching rate coefficient compared to that at room temperature. Figure 8 shows the total quenching rate coefficient can be described by simple Arrhenius behavior, $k(T) = 1.1 \times 10^{-10} \exp(-519 \pm 143\ K/T)$ and $E_a = 1.0$ kcal/mol. For comparison, collision theory gives the temperature dependence as $k(T) = 3.3 \times 10^{-12}\ T^{1/2} \exp(-302 \pm 135$ K/T) with $E_0 = 0.6$ kcal/mol. The only previous rate measurement for the $NCl(a^1\Delta) + I(^2P_{3/2})$ reaction is also included in Figure 8.

While the products of the $F/DCl/DI/HN_3$ reaction system (for example DF, HF) are slow quenchers of $NCl(a^1\Delta)$ and $I^*(^2P_{1/2})$ at room temperature, the possibility of an enhanced quenching effect of these species at higher temperatures is uncertain. To determine the extent of the collective quenching (by all flow

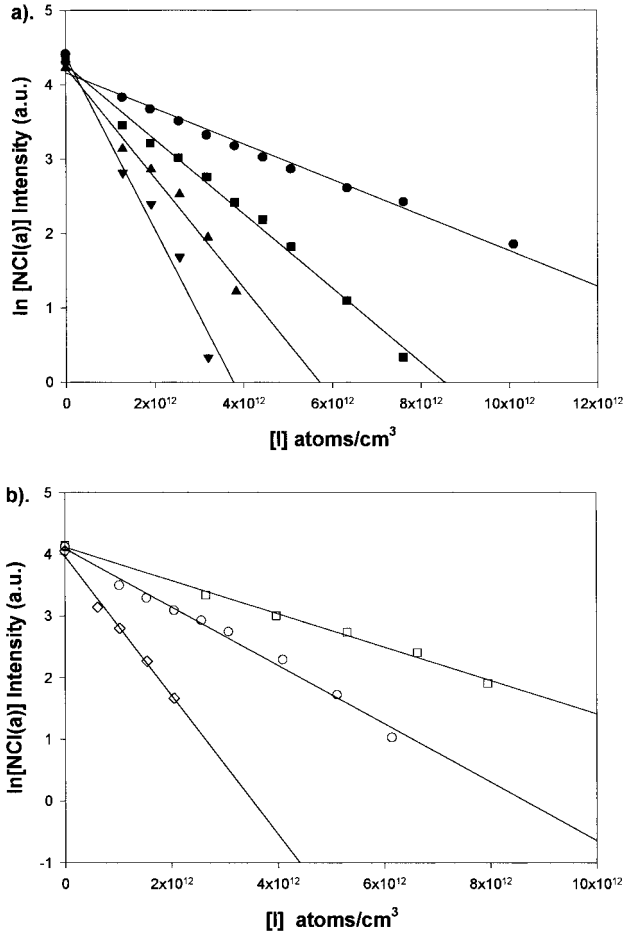

Figure 7. Quenching plots for NCl($a^1\Delta$) by I($^2P_{3/2}$) at elevated temperatures: (a) 345 K, $k_Q = (2.6 \pm 0.5) \times 10^{-11}$ cm^3/(molecule s); (b) 448 K, $k_Q = (4.1 \pm 0.6) \times 10^{-11}$ cm^3/(molecule s). The rate coefficients reflect a small positive change in the total quenching rate coefficient compared to that at room temperature.

TABLE 2: Summary of the *k*(*T*) Measurements over the 298−482 K Temperature Range

T (K)	*k*(*T*), 10^{-11} cm^3/(molecule s)	*T* (K)	*k*(*T*), 10^{-11} cm^3/(molecule s)
298	2.1 ± 0.6	384	2.8 ± 0.4
321	2.7 ± 1.0	403	3.4 ± 0.5
327	2.2 ± 0.7	438	3.3 ± 0.4
331	2.3 ± 0.2	448	4.1 ± 1.0
345	2.9 ± 0.5	457	3.7 ± 0.4
349	2.5 ± 0.9	473	3.4 ± 0.6
355	2.5 ± 0.9	482	3.6 ± 0.7

tube species) on NCl($a^1\Delta$) and I*($^2P_{1/2}$) in the heated flow tube, the reactor temperature was elevated and integrated NCl($a^1\Delta$) and I*($^2P_{1/2}$) intensities were collected. In these experiments a stable flow of F, DCl, HN_3, and DI was maintained at a constant pressure while the NCl($a^1\Delta$) and I*($^2P_{1/2}$) spectra were collected at a reaction time (corrected for temperature) corresponding to their maximum intensity in their respective time profiles. The effect of heating on the NCl($a^1\Delta$) and I*($^2P_{1/2}$) integrated intensity is shown in Figure 9 over the course of a 300−478 K range. It is apparent over this range the NCl($a^1\Delta$) and I*($^2P_{1/2}$) intensities remain approximately constant thus indicating that secondary side reactions do not enhance the quenching or diminish the formation of NCl($a^1\Delta$) and I*($^2P_{1/2}$). However, it should be noted that, after several days of reactor operation, the NCl($a^1\Delta$) and I*($^2P_{1/2}$) signals would gradually diminish to less than 10% over their original levels at all temperatures. This behavior is attributed to the formation of an unidentified

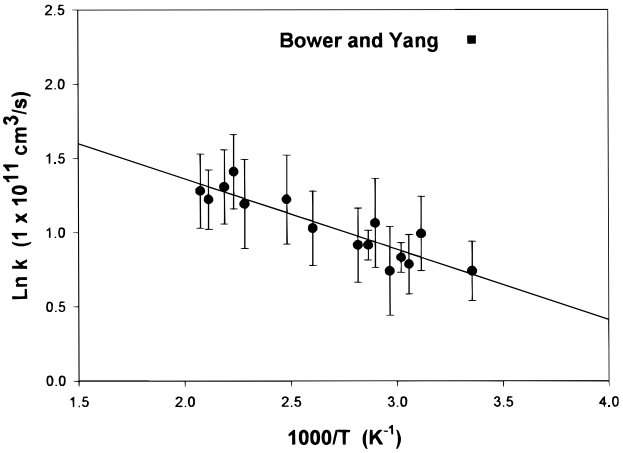

Figure 8. Total quenching rate coefficient for the NCl($a^1\Delta$) + I($^2P_{3/2}$) reaction for the temperature range of 300−482 K. The temperature dependence can be described by simple Arrhenius behavior, $k(T) = 1.0 \times 10^{-10} \exp(-519 \pm 143\ \mathrm{K}/T)$. A previous rate measurement (■) for the NCl($a^1\Delta$) + I($^2P_{3/2}$) reaction is also included.

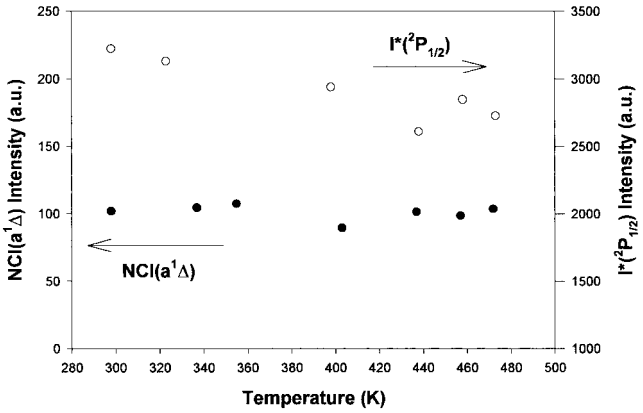

Figure 9. Effect of heating on the NCl($a^1\Delta$) and I*($^2P_{1/2}$) intensity over the course of the 300−478 K temperature range. Both NCl($a^1\Delta$) (●) and I*($^2P_{1/2}$) (○) intensities remain approximately constant across this temperature range indicating the stability of these metastables to quenching in the elevated temperature environment.

quencher species (presumably an iodine compound) on the reactor walls over time. The NCl($a^1\Delta$) and I*($^2P_{1/2}$) signals can be returned to their previous levels by ultrasonic cleaning of the reactor surfaces.

One important aspect in the evaluation of the NCl($a^1\Delta$)−I* laser system involves the relative efficiency of the I*($^2P_{1/2}$) production with respect to all other product channels:

$$\mathrm{NCl}(a^1\Delta) + \mathrm{I}(^2P_{3/2}) \rightarrow \mathrm{I}^*(^2P_{1/2}) + \mathrm{NCl}(X^3\Sigma^-) \qquad \Delta H = -1677\ \mathrm{cm}^{-1} \quad (19a)$$

$$\rightarrow \mathrm{I}(^2P_{3/2}) + \mathrm{NCl}(X^3\Sigma^-) \qquad \Delta H = -9280\ \mathrm{cm}^{-1} \quad (19b)$$

$$\rightarrow \text{other products} \quad (19c)$$

where the exoergicity of reaction 19 are based on a T_0 for NCl($a^1\Delta$)[28] = 9280 cm^{-1} and for I($^2P_{1/2}$) = 7603 cm^{-1}. Using the values for the excited-state I* formation rate coefficient and the total quenching rate coefficient determined above, an estimation of the I*($^2P_{1/2}$) product branching fraction at 300 K is given by $\phi \leq k_{I^*}/k_Q$. Accordingly, $\phi \leq 0.71$ and suggests the I($^2P_{3/2}$) atom efficiently extracts the energy from the NCl($a^1\Delta$) metastable, an outcome confirmed recently by Ray and

Coombe[5] in the photolytic $I^*(^2P_{1/2})$ laser demonstration-based $NCl(a^1\Delta) + I$ reaction. The branching ratio would be anticipated to be high since putting electronic energy into translation, reaction 19b, is not expected to be an efficient process. Even though the $I^*(^2P_{1/2})$ yield is high, there exists a probability of atom interchange based on the thermochemically[29,30] allowed reactive product channel

$$NCl(a^1\Delta) + I(^2P_{3/2}) \rightarrow ICl(X^1\Sigma) + N(^4S) \qquad \Delta H = -455\ \text{cm}^{-1} \quad (19d)$$

or perhaps

$$NCl(a^1\Delta) + I(^2P_{3/2}) \rightarrow Cl(^2P_{3/2}) + NI(X^3\Sigma) \quad (19e)$$

Although the ΔH°_f for NI is unknown and the reaction 19e thermochemistry is uncertain, the observation of matrix-isolated $NI(b^1\Sigma^+ - X^3\Sigma^-)$ fluorescence provides a convenient diagnostic tool for confirming the presence of NI.[31] Thus a product analysis of reactions 19a−e would be beneficial toward a more complete understanding of the quenching process. In particular, the identification of ICl or NI products would infer a chemical (reactive) quenching process occurs in addition to physical quenching.

Summary and Conclusion

The total quenching of $NCl(a^1\Delta)$ by $I(^2P_{3/2})$ over the 298−482 K temperature range shows an Arrhenius behavior with $k(T) = 1.1 \times 10^{-10} \exp(-519 \pm 143\ \text{K}/T)$. On the basis of the magnitude of the total quenching and energy transfer rate coefficients, the reaction appears to proceed efficiently to produce $I^*(^2P_{1/2})$ with a relatively high yield. Although the presence of $NF(a^1\Delta)$ and the moderately slow rise time of $NCl(a^1\Delta)$ suggest the $Cl + N_3$ reaction is slower than previously reported, the $Cl + N_3$ reaction represents a rapid and efficient means of generating $NCl(a^1\Delta)$. Using a simple kinetic model that simulated the experimental time histories of $NF(a^1\Delta)$ and $NCl(a^1\Delta)$ in this system, an estimated rate coefficient of $(1.6 \pm 0.4) \times 10^{-11}$ cm^3/(molecule s) for the $Cl + N_3$ reaction is determined with an $NCl(a^1\Delta)$ branching fraction ≥ 0.7. The complication of F atoms with the $Cl + N_3$ reaction can possibly be overcome by using alternative $NCl(a^1\Delta)$ reaction schemes such as the $Cl + HN_3$ reaction at elevated temperatures or the $H + NCl_3$ reaction system. Future work will be directed at measuring the $NCl(a^1\Delta)$ branching fraction and probing the reaction products for ICl(X) and NCl(X, $v'' = 2$) as a means of specifying the energy transfer mechanism.

Acknowledgment. This work was supported by the U.S. Air Force Office of Scientific Research. The authors are grateful for the helpful discussions with Profs. R. D. Coombe and D. W. Setser.

References and Notes

(1) Bower, R. D.; Yang, T. T. *J. Opt. Soc. Am. B* **1991**, *8*. 1583. There appears to be a misprint in the analysis of the NCl(a) + I quenching rate coefficient reported in Bower and Yang. Derivations of the quenching ratios obtained from Figures 6−8 support a slope to intercept ratio of 8.3×10^{-13}, 3.9×10^{-13}, and 3.8×10^{-13} for quenching by I, O_2, and Cl_2, respectively. This translates into a relative quenching rate coefficient of k_I:k_{O_2}:k_{Cl_2} of 2:1:1 and a rate coefficient of $k > 1 \times 10^{-11}$ cm^3/molecule s.

(2) Yang, T. T.; Gylys, V. T.; Bower, R. D.; Rubin, L. F. *Opt. Lett.* **1992**, *24*, 1803.

(3) Ray, A. J.; Coombe, R. D. *J. Phys. Chem.* **1993**, *97*, 3457.

(4) Ray, A. J.; Coombe, R. D. *J. Phys. Chem.* **1994**, *98*, 8940.

(5) Ray, A. J.; Coombe, R. D. *J. Phys. Chem.* **1995**, *99*, 7849.

(6) (a) Exton, D. B.; Gilbert, J. V.; Coombe, R. D. *J. Phys. Chem.* **1991**, *95*, 2692. (b) Schwenz, R. W.; Gilbert, J. V.; Coombe, R. D. *Chem. Phys. Lett.* **1993**, *207*, 526. (c) Singleton, S. M.; Coombe, R. D. *Chem. Phys. Lett.* **1993**, *215*, 237.

(7) The calibration curve for a Hamamatsu R1767 photomultiplier tube coupled to a 1 m fl monochromator with a 1 μm blaze, 600 grooves/mm grating was gratefully provided by D. W. Setser.

(8) Benard, D. J.; Chowdhury, M. A.; Winker, B. K.; Seder, T. A.; Michels, H. H. *J. Phys. Chem.* **1990**, *94*, 7507.

(9) Liu, X.; MacDonald, M. A.; Coombe, R. D. *J. Phys. Chem.* **1992**, *96*, 4907.

(10) (a) Clyne, M. A. A.; MacRobert, A. J.; Brunning, J.; Cheah, C. T. *J. Chem. Soc., Faraday Trans. 2* **1983**, *79*, 1515. (b) Pritt, A. T., Jr.; Coombe, R. D. *Int. J. Chem. Kinet.* **1980**, *12*, 741.

(11) Henshaw, T. L.; Herrera, S. D.; Haggquist, G. W.; Schlie, L. A. *J. Phys. Chem.* **1997**, *101*, 4048.

(12) Du, K. Y.; Setser, D. W. *J. Phys. Chem.* **1990,** *94*, 2425.

(13) Clyne, M. A. A.; Nip, W. S. *J. Chem. Soc., Faraday Trans. 2* **1977**, *73*, 1308.

(14) Habdas, J.; Wategaonkar, S.; Setser, D. W. *J. Phys. Chem.* **1987**, *91*, 451.

(15) Mei, C. C.; Moore, C. B. *J. Chem. Phys*. **1977**, *67*, 3936.

(16) Private communication with R. D. Coombe, 1997.

(17) Quiones, E.; Habdas, J.; Setser, D. W. *J. Phys. Chem*. **1987**, *91*, 5155.

(18) Private communication with D. W. Setser, 1997.

(19) Alexander, M. H.; Werner, H. J.; Hemmer, T.; Knowles, P. J. *J. Chem. Phys*. **1990**, *93*, 3307.

(20) Schmidt, M. W.; Gordon, M. S.; Dupuis, M. J. *J. Am. Ceram. Soc*. **1985**, *107*, 2585.

(21) Kajimoto, O.; Yamamoto, T. *J. Phys. Chem*. **1979**, *83*, 429.

(22) Benard, D. J.; Winker, B. K.; Chowdhury, M. A.; Seder, T. A.; Michels, H. H. Unpublished data.

(23) Habdas, J.; Setser, D. W. *J. Phys. Chem.* **1989**, *93*, 229.

(24) Malins, R. J.; Setser, D. W. *J. Phys. Chem.* **1981**, *85*, 1342.

(25) Becker, A. C.; Schurath, U.; *Chem. Phys. Lett.* **1989**, *160*, 586.

(26) Yarkony, D. R. *J. Chem. Phys.* **1987**, *86*, 1642.

(27) Betterdorff, M.; Klotz, R.; Peyerimhoff, S. D. *Chem. Phys.* **1986**, *110*, 315.

(28) Pritt, A. T.; Patel, D.; Coombe, R. D. *J. Molec. Spectrosc*. **1981**, *87*, 401.

(29) In this calculation we adopt the most recent *ab initio* value of D_e = 76.6 kcal/mol for $NCl(X^1\Sigma^-)$: Xantheas, S. S.; Dunning, T. H., Jr.; Marvridis, A. *J. Chem. Phys*. **1997**, *106*, 3280.

(30) Chase, M. W.; Curnutt, J. L.; Prophet, H.; Syverud, A. N.; Walker, L. C.; JANAF Thermochemical Tables, 1975 Supplement. *J. Phys. Chem. Ref. Data* **1975**, *4*, 1.

(31) Becker, A. C.; Langen, J.; Oberhoffer, H. M.; Schurath, U. *J. Chem. Phys.* **1986**, *84*, 2907.